Steel and Composite Structures, *Vol. 29, No. 3 (2018) 363-377*
DOI: https://doi.org/10.12989/scs.2018.29.3.363

Free vibration of tapered BFGM beams using an efficient shear deformable finite element model

Dinh Kien Nguyen [*1,2] and Thi Thom Tran [1,2a]

[1] *Institute of Mechanics, VAST, 18 Hoang Quoc Viet, Hanoi, Vietnam*
[2] *Graduate University of Science and Technology, VAST, 18 Hoang Quoc Viet, Hanoi, Vietnam*

(*Received May 11, 2018, Revised August 22, 2018, Accepted September 25, 2018*)

Abstract. An efficient and free of shear locking finite element model is developed and employed to study free vibration of tapered bidirectional functionally graded material (BFGM) beams. The beam material is assumed to be formed from four distinct constituent materials whose volume fraction continuously varies along the longitudinal and thickness directions by power-law functions. The finite element formulation based on the first-order shear deformation theory is derived by using hierarchical functions to interpolate the displacement field. In order to improve efficiency and accuracy of the formulation, the shear strain is constrained to constant and the exact variation of the cross-sectional profile is employed to compute the element stiffness and mass matrices. A comprehensive parametric study is carried out to highlight the influence of the material distribution, the taper and aspect ratios as well as the boundary conditions on the vibration characteristics. Numerical investigation reveals that the proposed model is efficient, and it is capable to evaluate the natural frequencies of BFGM beams by using a small number of the elements. It is also shown that the effect of the taper ratio on the fundamental frequency of the BFGM beams is significantly influenced by the boundary conditions. The present results are of benefit to optimum design of tapered FGM beam structures.

Keywords: bi-directional functionally graded material; tapered beams; first-order shear deformation theory; hierarchical functions; free vibration; finite element model

1. Introduction

Functionally graded materials (FGMs) initiated by Japanese scientists in the middle eighties as space materials are increasingly used for development of structural elements subjected to severe mechanical and thermal loading (Birman and Byrd 2007). Beam as a major part in many structures is designed to resist different static and dynamic loading, and new materials, including composites and FGMs are increasingly employed to fabricate this important structural element for improving its strength to weight ratio. Investigation on mechanical behavior of FGM beams has drawn much attention from researchers in recent years, and a large number of publications on static (Chakraborty *et al*. 2003, Kadoli *et al*. 2008, Frikha *et al*. 2016), vibration (Li 2008, Li *et al*. 2013, Mahi *et al*. 2010, Trinh *et al*. 2016), and buckling (Wattanasakulpong *et al*. 2011, Kahya and Turan 2017) behavior of FGM beams have been reported in the literature.

Non-prismatic beams with variable cross section are important in engineering because of their ability in optimizing the weight and strength of structures. Due to the variable coefficients in the governing differential equations, analytical methods are often encountered difficulties in analyzing the variable cross section beams, and a special technique or a numerical method should be employed instead of. In this line of works, Huang and Li (2010) studied free vibration of axially FGM Euler-Bernoulli beams with variable flexural rigidity and mass density by transforming the governing equations to Fredholm integral equations and expanding the mode shape into power series. The authors then extended the study to buckling analysis of axially graded Euler-Bernoulli beams with arbitrarily axial varying cross section (Huang and Li 2011). An auxiliary function for transforming the couple governing equations to a single governing differential equation was introduced by Huang *et al*. (2013) for determining natural frequencies of axially FGM Timoshenko beams. The proposed method is capable to determine the lower and higher natural frequencies simultaneously from the multi-roots. Tang *et al*. (2014) derived the exact frequency equations for free vibration of non-uniform FGM Timoshenko beams with bending stiffness and mass density longitudinally varying by an exponential law. The free vibration of non-uniform axially FGM beams was also considered by Hein and Feklistova (2011) by using Haar wavelet method. Based on Timoshenko beam theory, Shahba *et al*. (2011) formulated a finite beam element for free vibration and stability analysis of tapered axially FGM beams with classical and non-classical boundary conditions. The element employed the solution of static part of governing equations to interpolate the displacement field, which helps to improve its convergence. Shahba and Rajasekaran (2012) employed the

*Corresponding author, Ph.D., Associate Professor,
E-mail: ndkien@imech.vast.vn
[a] Ph.D. Student

ISSN: 1229-9367 (Print), 1598-6233 (Online)

differential transform method (DTM) and differential quadrature method (DQM) to study free vibration and stability of axially FGM Euler-Bernoulli beams. The modified couple stress theory and Rayleigh–Ritz method were used by Akgöz and Civalek (2013) to determine natural frequencies of tapered axially FGM microbeams. Rajasekaran (2013), Rajasekaran and Tochaei (2014) employed DTM to study the buckling and vibration of tapered beams formed from axially FGM. The authors showed that the DTM is able to capture the effects of variable cross section, centrifugal force and the material inhomogeneity, and the tapered ratio has decreasing the effect on natural frequencies of the beams. The co-rotational finite element formulations (Nguyen 2013, Nguyen and Gan 2014), and the generalized DQM (Niknam *et al*. 2014) were used to study large deflection behavior of tapered beams with the material properties varying in the thickness or longitudinal direction. Gan *et al*. (2015) derived a finite element formulation for studying the vibration of Timoshenko beams under multiple moving loads. The cross section of the beams was considered to be linear variation along the beam length and the material properties are assumed to vary in the axial direction by a power- law function. The DQM was utilized in combination with the domain decomposition technique by Bambill *et al*. (2015) to study free vibration of stepped axially FGM Timoshenko beams. Different combinations of classical and elastic boundary conditions have been considered in the work. Also using the DQM, Ghazaryan *et al*. (2017) carried out a free vibration analysis of FGM beams with non-uniform cross section. Calim (2016) applied complementary function method in transient analysis of axially FGM Timoshenko beam with variable cross section. The dynamic response of tapered beams under impulsive load was obtained by the author by using the modified Durbin's algorithm. B-spline method was employed by Li and Zhang (2015) in dynamic analysis of rotating AFG beams with linearly varying cross section. Recently, Zhao *et al*. (2017) considered free vibration of axially FGM beams with varying cross section by using Chebyshev polynomials theory.

The FGM beams in the above discussed references are formed from unidirectional FGMs with material properties varying in one spatial direction, axial or transverse direction only. The unidirectional FGMs may not be appropriate to resist multi-directional variations of thermal and mechanical loadings in many practical circumstances. For example, the temperature on the outer surface of the new aerospace craft in sustained flight can range from 1033K along the top of the fuselage to 2066K at the nose and from outer surface temperature to room temperature inside the plane (Nemat-Alla and Noda 2000). Development of FGMs with effective material properties varying in two or three directions for withstanding severe general loadings, therefore is great important. Analysis of beams made of bi-directional functionally graded material (BFGM) has been carried out by several authors in recent years. Using a hybrid state space-based DQM, Lü *et al*. (2008) derived semi-analytical elasticity solutions for static bending and thermal deformation of BFGM beams with Young's modulus varying exponentially along the thickness and longitudinal directions. The exponential variation of material properties was also considered by Simşek (2015) in vibration analysis of BFGM beams under a moving load. The author showed that the natural frequencies and dynamic response of the beams are significantly influenced by the material gradient distribution, and the material properties of the BFGM beams can be selected to meet the design goals of optimizing the dynamic response. The forced vibration of FGM Timoshenko beams with material properties varying exponentially in both the thickness and length directions was also studied by the dynamic stiffness method (Hao and Wei 2016). The NURBS isogeometric finite element approach was employed by Lezgy-Nazargah (2015), Huynh *et al*. (2017) to investigate the coupled thermo-mechanical behavior and free vibration of BFGM beams, respectively. Wang *et al*. (2016) assumed the material properties following an exponential function along the beam length and a power-law function though the thickness in the free vibration analysis of BFGM Euler-Bernoulli beams. Numerical investigation in the work showed that there is a critical frequency at which the natural frequencies have an abrupt jump. Nguyen *et al*. (2017) considered the forced vibration of BFGM beams formed from four distinct constituent materials whose volume fraction varying in both the thickness and longitudinal directions by power functions. A first-order shear deformable finite element formulation was derived by the authors for computing the dynamic response of the beams carrying a moving load. Based on the classical hairbrush hypothesis, Pydah and Sabale (2017) presented an analytical model for static bending analysis of circular FGM beams with material properties varying smoothly along tangential and radial directions. Karamanli (2017) studies bending behavior of BFGM sandwich beams by using the quasi-3D shear deformation theory and the symmetric smoothed particle hydrodynamics method. The generalized DQM has been employed by Shafiei and Kazemi (2017), Shafiei *et al*. (2017) to study buckling and vibration of porous BFGM nano/micro beams, respectively. Based on a quasi-3D theory, Trinh *et al*. (2018) studied free vibration of BFGM mirobeams by assuming the material properties to vary exponentially along both longitudinal and thickness directions.

In this paper, the free vibration analysis of tapered BFGM beams using a finite element procedure is presented. The beams are considered to be formed from four distinct constituent materials whose volume fraction varying in the thickness and longitudinal directions by power-law functions. A first-order shear deformable finite element model using hierarchical functions to interpolate displacement field is derived and employed in the analysis. To improve the accuracy and efficiency of the finite element formulation, the shear strain is constrained to constant and the exact variation of the cross-sectional profile is employed to evaluate the element stiffness and mass matrices. Validation of the model is confirmed by comparing the numerical results of the present work with the published data. A parametric study is carried out to highlight the effects of the material distribution and taper ratio of

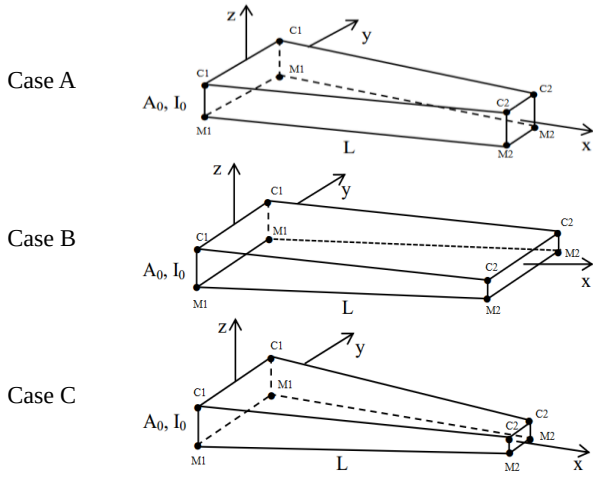

Fig. 1 Geometry and coordinate system of FGM beams for different tapered cases

vibration characteristics. The influence of the aspect ratio on the frequencies of the beams is also examined and discussed.

2. Tapered BFGM beam

An FGM beam with rectangular cross section and length of L is considered. The beam is assumed to be longitudinally tapered in three following taper cases

$$\begin{aligned}
&\text{Case A:}\quad A(x)=A_0\left(1-\alpha\frac{x}{L}\right),\quad I(x)=I_0\left(1-\alpha\frac{x}{L}\right)\\
&\text{Case B:}\quad A(x)=A_0\left(1-\alpha\frac{x}{L}\right),\quad I(x)=I_0\left(1-\alpha\frac{x}{L}\right)^3\\
&\text{Case C:}\quad A(x)=A_0\left(1-\alpha\frac{x}{L}\right)^2,\quad I(x)=I_0\left(1-\alpha\frac{x}{L}\right)^4
\end{aligned}\tag{1}$$

where $A(x)$ and $I(x)$ are, respectively, the area and inertia moment of cross section; A_0 and I_0 are the area and moment of inertia of the section at the left end ($x = 0$), respectively; $0 \le \alpha < 1$ is the taper ratio. The beam become uniform when $\alpha = 0$. The three tapered cases are illustrated in Fig. 1, where the Cartesian coordinate system (x, y, z) is chosen such that the x-axis is on the mid-plane and z-axis directs along the thickness direction.

The beam material is assumed to be formed from two ceramics, referred to as ceramic 1 (C1) and ceramic 2 (C2), and two metals, referred to as metal 1 (M1) and metal 2 (M2), whose volume fraction varies in both the thickness and longitudinal directions according to

$$\begin{aligned}
V_{C1}&=\left(\frac{z}{h}+\frac{1}{2}\right)^{n_z}\left[1-\left(\frac{x}{L}\right)^{n_x}\right],\\
V_{C2}&=\left(\frac{z}{h}+\frac{1}{2}\right)^{n_z}\left(\frac{x}{L}\right)^{n_x},\\
V_{M1}&=\left[1-\left(\frac{z}{h}+\frac{1}{2}\right)^{n_z}\right]\left[1-\left(\frac{x}{L}\right)^{n_x}\right],\\
V_{M2}&=\left[1-\left(\frac{z}{h}+\frac{1}{2}\right)^{n_z}\right]\left(\frac{x}{L}\right)^{n_x}
\end{aligned}\tag{2}$$

where n_x and n_z are the material grading indexes, which dictate the variation of the constituent materials along the x and z directions, respectively. It can be seen from Eq. (2) that the left and right lower sides, corresponding to ($x = 0$, $z = -h/2$) and ($x = L$, $z = -h/2$), contain only M1 and M2, respectively, whereas the corresponding upper two sides, according to ($x = 0$, $z = h/2$) and ($x = L$, $z = h/2$) are, respectively, pure C1 and C2. The variation of the volume fraction of C1 and C2 in the x- and z-directions according to Eq. (2) is depicted in Fig. 2 for various values of the material grading indexes n_x and n_z.

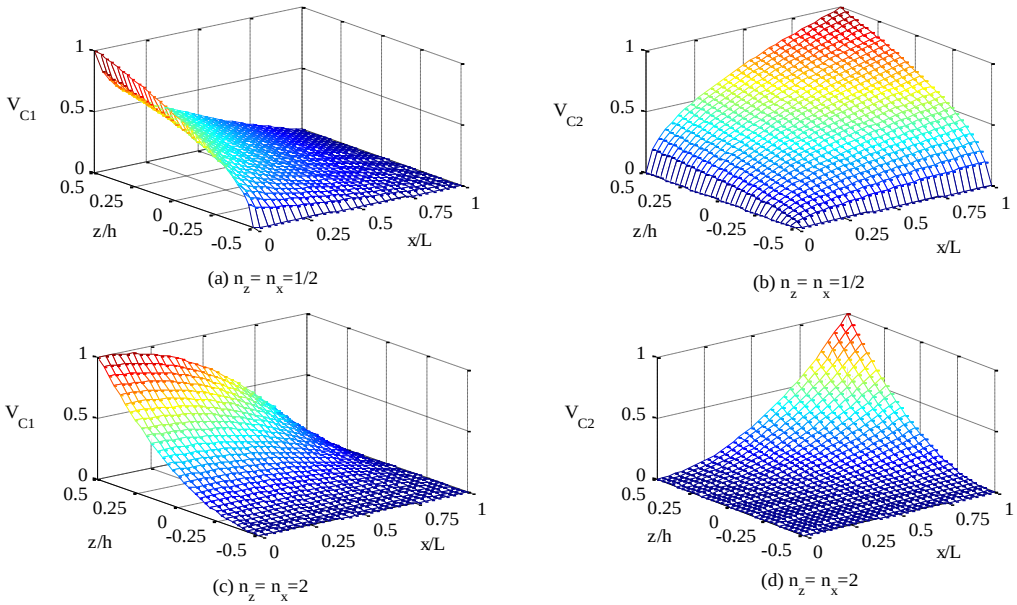

Fig. 2 Variation of volume fraction of ceramics in the longitudinal and thickness directions

Effective material properties P such as the elastic modulus and the mass density are evaluated according to

$$\mathrm{P} = V_{C1}\mathrm{P}_{C1} + V_{C2}\mathrm{P}_{C2} + V_{M1}\mathrm{P}_{M1} + V_{M2}\mathrm{P}_{M2} \tag{3}$$

where P_{c1}, P_{c2}, P_{M1} and P_{M2} denote the properties of the C1, C2, M1 and M2, respectively.

Using Eq. (2), one can rewrite Eq. (3) in the form

$$\begin{aligned}\mathrm{P}(x,z) = &\left[\left(\mathrm{P}_{C1}-\mathrm{P}_{M1}\right)\left(\frac{z}{h}+\frac{1}{2}\right)^{n_z}+\mathrm{P}_{M1}\right]\left[1-\left(\frac{x}{L}\right)^{n_x}\right]\\ &+\left[\left(\mathrm{P}_{C2}-\mathrm{P}_{M2}\right)\left(\frac{z}{h}+\frac{1}{2}\right)^{n_z}+\mathrm{P}_{M2}\right]\left(\frac{x}{L}\right)^{n_x}\end{aligned} \tag{4}$$

It is evident that Eq. (4) deduces to the effective material properties of a unidirectional transverse FGM beam if n_x = 0, or if C1 is the same as C2, and M1 is identical to M2. In addition, if n_z = 0, Eq. (4) results in the effective material properties of an axially FGM beam formed from C1 and C2.

Based on the first-order shear deformation theory, the axial displacement, $u_1(x, z, t)$, and transverse displacement, $u_3(x, z, t)$, at any point of the beam are given by

$$\begin{aligned}u_1(x,z,t) &= u(x,t) - z\theta(x,t)\\ u_3(x,z,t) &= w(x,t)\end{aligned} \tag{5}$$

where z is the distance from the mid-plane to the considering point; $u(x,t)$ and $w(x,t)$ are, respectively, the axial and transverse displacements of the point on the mid-plane; $\theta(x,t)$ is the cross-sectional rotation.

The axial strain (ε_{xx}) and the shear strain (γ_{xz}) resulted from Eq. (4) are of the forms

$$\begin{aligned}\varepsilon_{xx} &= u_{,x} - z\theta_{,x},\\ \gamma_{xz} &= w_{,x} - \theta\end{aligned} \tag{6}$$

where and hereafter, a subscript comma is used to indicate the derivative of the variable with respect to the spatial coordinate x.

The constitutive relation for the BFGM beam based on Hooke's law is of the form

$$\begin{aligned}\sigma_{xx} &= E(x,z)\,\varepsilon_{xx},\\ \tau_{xz} &= G(x,z)\,\gamma_{xz}\end{aligned} \tag{7}$$

where σ_{xx} and τ_{xz} are the axial and shear stresses, respectively; $E(x,z)$ and $G(x,z)$ are, respectively, the Young's modulus and shear modulus, and they are functions of both the spatial coordinates, x and z.

The strain energy of the beam (U) resulted from (6) and (7) is as follows

$$\begin{aligned}U &= \frac{1}{2}\int_0^L\int_{A(x)}\left(\sigma_{xx}\varepsilon_{xx}+\tau_{xz}\gamma_{xz}\right)dAdx\\ &= \frac{1}{2}\int_0^L\Big[A_{11}u_{,x}^2 - 2A_{12}u_{,x}\theta_{,x} + A_{22}\theta_{,x}^2\\ &\qquad + \psi A_{33}\left(w_{,x}-\theta\right)^2\Big]\end{aligned} \tag{8}$$

where ψ is the shear correction factor, chosen by 5/6 for the beams with rectangular cross section considered herein; A_{11}, A_{12}, A_{22} and A_{33} are, respectively, the extensional, extensional-bending coupling, bending rigidities and shear rigidity, which are defined as

$$\begin{aligned}\left(A_{11}, A_{12}, A_{22}\right)(x,z) &= \int_{A(x)} E(x,z)\left(1, z, z^2\right)dA,\\ A_{33}(x,z) &= \int_{A(x)} G(x,z)\,dA\end{aligned} \tag{9}$$

with the cross-sectional area $A(x)$ is defined in Eq. (1).

Using Eq. (4), one can rewrite the beam rigidities in (9) as follows

$$\begin{aligned}A_{11}(x,z) &= A_{11}^{C1M1} - \left(A_{11}^{C1M1} - A_{11}^{C2M2}\right)\left(\frac{x}{L}\right)^{n_x},\\ A_{12}(x,z) &= A_{12}^{C1M1} - \left(A_{12}^{C1M1} - A_{12}^{C2M2}\right)\left(\frac{x}{L}\right)^{n_x},\\ A_{22}(x,z) &= A_{22}^{C1M1} - \left(A_{22}^{C1M1} - A_{22}^{C2M2}\right)\left(\frac{x}{L}\right)^{n_x},\\ A_{33}(x,z) &= A_{33}^{C1M1} - \left(A_{33}^{C1M1} - A_{33}^{C2M2}\right)\left(\frac{x}{L}\right)^{n_x}\end{aligned} \tag{10}$$

where A_{11}^{C1M1}, A_{12}^{C1M1}, A_{22}^{C1M1} and A_{33}^{C1M1} are the rigidities of the unidirectional transverse FGM beam formed from C1 and M1; A_{11}^{C2M2}, A_{12}^{C2M2}, A_{22}^{C2M2} and A_{33}^{C2M2} are the rigidities of the transverse FGM beam composed of C2 and M2. As can be clearly seen again from Eq. (10) that the rigidities of the present BFGM beam degenerate to that of the unidirectional FGM beam if n_x = 0 or the two ceramics and two metals are identical. Since A_{ij}^{C1M1}, A_{ij}^{C2M2} are functions of z only, explicit expressions for these rigidities can easily be obtained (Nguyen *et al*. 2017).

The kinetic energy for the beam (T) resulted from Eq. (5) is of the form

$$\begin{aligned}\mathrm{T} &= \frac{1}{2}\int_0^L\int_{A(x)}\rho(x,z)\left(\dot{u}_1^{\,2}+\dot{u}_3^{\,2}\right)dAdx\\ &= \frac{1}{2}\int_0^L\Big[I_{11}\left(\dot{u}^2+\dot{w}^2\right) - 2I_{12}\dot{u}\dot{\theta} + I_{22}\dot{\theta}^2\Big]\,dx\end{aligned} \tag{11}$$

where an over dot is used to indicate the differentiation with respect to time variable t, and I_{11}, I_{12}, I_{22} are the mass moments, defined as

$$\left(I_{11}, I_{12}, I_{22}\right) = \int_{A(x)}\rho(x,z)\left(1, z, z^2\right)dA \tag{12}$$

The mass moments can be also written in the form

$$\begin{aligned}I_{11}(x,z) &= I_{11}^{C1M1} - \left(I_{11}^{C1M1} - I_{11}^{C2M2}\right)\left(\frac{x}{L}\right)^{n_x},\\ I_{12}(x,z) &= I_{12}^{C1M1} - \left(I_{12}^{C1M1} - I_{12}^{C2M2}\right)\left(\frac{x}{L}\right)^{n_x},\\ I_{22}(x,z) &= I_{22}^{C1M1} - \left(I_{22}^{C1M1} - I_{22}^{C2M2}\right)\left(\frac{x}{L}\right)^{n_x}\end{aligned} \tag{13}$$

with I_{ij}^{C1M1} (i, j = 1, 2) denote the mass moments of the unidirectional FGM beams formed from C1 and M1, and I_{ij}^{C2M2} are the corresponding mass moments of the beam formed from C2 and M2, respectively.

Equations of motion for the BFGM beam can be obtained by applying Hamilton's principle to Eqs. (8) and (11), and they have the following forms

$$\begin{cases} I_{11}\ddot{u} - I_{12}\ddot{\theta} - \left(A_{11}u_{,x} - A_{12}\theta_{,x}\right)_{,x} = 0 \\ I_{11}\ddot{w} - \psi\left[A_{33}\left(w_{,x} - \theta\right)\right]_{,x} = 0 \\ I_{12}\ddot{u} - I_{22}\ddot{\theta} - \left(A_{12}u_{,x} - A_{22}\theta_{,x}\right)_{,x} \\ \qquad + \psi A_{33}\left(w_{,x} - \theta\right) = 0 \end{cases} \tag{14}$$

It is necessary to note that the coefficients of the above differential equations are functions of both x and z, and thus a closed-form solution is difficult to obtain. A finite element model is developed herein to solve Eq. (14).

3. Finite element model

This section derives the finite element formulation, namely the stiffness and mass matrices for a beam element with length of l. A first-order shear deformable finite beam formulation can be formulated using linear functions with reduced integration technique to avoid the shear locking (Cook *et al*. 2002). The formulation derived from the linear functions is, however slow convergence. Convergence of a first-order finite element formulation can be improved by using the higher-order polynomials to interpolate the displacement field as shown by Nguyen *et al*. (2017). The finite element formulation derived from the higher-order polynomials, however has a drawback. Since the coefficients of the polynomials are determined from the element boundary conditions, related to nodal values of the variables, totally new shape functions have to be re-determined whenever the mesh refinement is made. A finite element formulated from the hierarchical functions, in which the higher-order shape functions contain the lower-order ones, enables to overcome the above drawback (Zienkiewicz and Taylor 1997). The hierarchical functions have been employed previously by Nguyen and Bui (2017) to formulate a unidirectional FGM Timoshenko beam element, and they are used herein to derive stiffness and mass matrices for the BFGM beam element. For one-dimensional beam, the hierarchical functions are of the forms (Zienkiewicz and Taylor 1997)

$$\begin{aligned} &N_1 = \frac{1}{2}(1-\xi),\ N_2 = \frac{1}{2}(1+\xi), \\ &N_3 = \left(1-\xi^2\right),\ N_4 = \xi\left(1-\xi^2\right) \end{aligned} \tag{15}$$

where $\xi = 2\frac{x}{l} - 1$ is the natural coordinate.

In the first-order shear deformable finite element beam model, a quadratic variation of the rotation should be chosen to represent a linearly varying bending moments along the element. With the shear strain given by Eq. (6), interpolation functions for the transverse displacement w should be chosen one order higher than that of the rotation θ. In this regard, the displacements and rotation can be interpolated as follows

$$\begin{aligned} u &= \frac{1}{2}(1-\xi)u_1 + \frac{1}{2}(1+\xi)u_2, \\ \theta &= \frac{1}{2}(1-\xi)\theta_1 + \frac{1}{2}(1+\xi)\theta_2 + \left(1-\xi^2\right)\theta_3, \\ w &= \frac{1}{2}(1-\xi)w_1 + \frac{1}{2}(1+\xi)w_2 + \left(1-\xi^2\right)w_3 \\ &\quad + \xi\left(1-\xi^2\right)w_4 \end{aligned} \tag{16}$$

where u_1, u_2, θ_1, θ_2, θ_3, w_1,..., w_4 are nine unknown values of the variables. Noting that θ_3, w_3 and w_4 are not values of the variables at the nodes.

The efficiency of the finite element formulation can be improved by constraining the shear strain γ_{xz} to constant, and the number of the unknown values reduces from nine to seven (Nguyen and Bui 2017). Substituting θ and w from Eq. (16) into expression for γ_{xz} in Eq. (6), one gets

$$\begin{aligned} \gamma_{xz} = &\left(-\frac{6}{l}w_4 + \theta_3\right)\xi^2 - \left(\frac{4}{l}w_3 - \frac{1}{2}\theta_1 + \frac{1}{2}\theta_2\right)\xi \\ &+ \left[\frac{1}{l}\left(w_2 - w_1 + 2w_4\right) - \frac{1}{2}\left(\theta_1 + \theta_2 + 2\theta_3\right)\right] \end{aligned} \tag{17}$$

By constraining γ_{xz} to constant, one gets

$$w_3 = \frac{l}{8}\left(\theta_1 - \theta_2\right), \text{ and } w_4 = \frac{l}{6}\theta_3 \tag{18}$$

Using (18), one can be rewrite Eq. (16) in the form

$$\begin{aligned} u &= \frac{1}{2}(1-\xi)u_1 + \frac{1}{2}(1+\xi)u_2, \\ \theta &= \frac{1}{2}(1-\xi)\theta_1 + \frac{1}{2}(1+\xi)\theta_2 + \left(1-\xi^2\right)\theta_3, \\ w &= \frac{1}{2}(1-\xi)w_1 + \frac{1}{2}(1+\xi)w_2 \\ &\quad + \frac{l}{8}\left(1-\xi^2\right)\left(\theta_1 - \theta_2\right) + \frac{l}{6}\xi\left(1-\xi^2\right)\theta_3 \end{aligned} \tag{19}$$

and the shear strain γ_{xz} is now of the form

$$\gamma_{xz} = \frac{1}{l}\left(w_2 - w_1\right) - \frac{1}{2}\left(\theta_1 + \theta_2\right) - \frac{2}{3}\theta_3 \tag{20}$$

The finite element formulation in the present work is formulated from seven unknown values u_1, u_2, w_1, w_2, θ_1, θ_2 and θ_3 with the interpolation scheme defined by Eq. (19). The vector of unknown values for a generic beam element is given by

$$\mathbf{d} = \left\{u_1\ w_1\ \theta_1\ \theta_3\ u_2\ w_2\ \theta_2\right\}^T \tag{21}$$

where u_i, w_i and θ_i (i = 1, 2) is the displacements and rotations at nodes 1 and 2, but θ_3 is not a nodal rotation.

Noting that the order of the unknown for the element vector is not necessary as that of Eq. (21).

The interpolation (19) can be written using the vector of unknown values as

$$u=\mathbf{N}_u\mathbf{d},\quad \theta=\mathbf{N}_\theta\mathbf{d},\quad w=\mathbf{N}_w\mathbf{d} \tag{22}$$

with

$$\begin{aligned}\mathbf{N}_u&=\{N_1\ \ 0\ \ 0\ \ 0\ \ N_2\ \ 0\ \ 0\}\\ \mathbf{N}_\theta&=\{0\ \ 0\ \ N_1\ \ N_3\ \ 0\ \ 0\ \ N_2\}\\ \mathbf{N}_w&=\left\{0\ \ N_1\ \ \frac{l}{8}N_3\ \ \frac{l}{6}N_4\ \ 0\ \ N_2\ \ -\frac{l}{8}N_3\right\}\end{aligned} \tag{23}$$

are the matrices of interpolation functions for u, θ and w, respectively.

With the interpolation scheme (22), the strain energy of the beam in Eq. (8) can be written in the form

$$U=\frac{1}{2}\sum_{i=1}^{ne}\mathbf{d}^T\mathbf{k}\,\mathbf{d},\ \text{with}\ \mathbf{k}=\mathbf{k}_{uu}+\mathbf{k}_{u\theta}+\mathbf{k}_{\theta\theta}+\mathbf{k}_{ss} \tag{23}$$

where ne is total number of the elements; $\mathbf{k}$ is the element stiffness matrix; $\mathbf{k}_{uu}$, $\mathbf{k}_{u\theta}$, $\mathbf{k}_{\theta\theta}$ and $\mathbf{k}_{ss}$ are, respectively, the element stiffness matrices stemming from the axial stretching, axial stretching-bending coupling, bending and shear deformation. Using Eq. (10), one can write these matrices $\mathbf{k}_{uu}$, $\mathbf{k}_{u\theta}$, $\mathbf{k}_{\theta\theta}$ and $\mathbf{k}_{ss}$ in the following forms

$$\begin{aligned}\mathbf{k}_{uu}&=\frac{2}{l}\int_{-1}^{1}\mathbf{N}_{u,\xi}^T\left[A_{11}^{C1M1}-A_{11}^{C12M12}\left(\frac{\xi+1}{2}\right)^{n_x}\right]\mathbf{N}_{u,\xi}d\xi,\\ \mathbf{k}_{u\theta}&=-\frac{2}{l}\int_{-1}^{1}\mathbf{N}_{u,\xi}^T\left[A_{12}^{C1M1}-A_{12}^{C12M12}\left(\frac{\xi+1}{2}\right)^{n_x}\right]\mathbf{N}_{\theta,\xi}d\xi,\\ \mathbf{k}_{\theta\theta}&=\frac{2}{l}\int_{-1}^{1}\mathbf{N}_{\theta,\xi}^T\left[A_{22}^{C1M1}-A_{22}^{C12M12}\left(\frac{\xi+1}{2}\right)^{n_x}\right]\mathbf{N}_{\theta,\xi}d\xi,\\ \mathbf{k}_{ss}&=\frac{l}{2}\int_{-1}^{1}\left(\frac{2}{l}\mathbf{N}_{w,\xi}^T-\mathbf{N}_\theta^T\right)\Big[\psi A_{33}^{C1M1}\\ &\quad-\psi A_{33}^{C12M12}\left(\frac{\xi+1}{2}\right)^{n_x}\Big]\left(\frac{2}{l}\mathbf{N}_{w,\xi}-\mathbf{N}_\theta\right)d\xi\end{aligned} \tag{25}$$

where notations $A_{11}^{C12M12}=A_{11}^{C1M1}-A_{11}^{C2M2}$, $A_{12}^{C12M12}=A_{12}^{C1M1}-A_{12}^{C2M2}$, $A_{22}^{C12M12}=A_{22}^{C1M1}-A_2^{C2M2}$, $A_{33}^{C12M12}=A_{33}^{C1M1}-A_{33}^{C2M2}$ have been used. In order to improve the accuracy of the finite element formulation, the exact variation of the cross-sectional profile is employed to evaluate the stiffness matrices in Eq. (25).

Similarly, the kinetic energy (11) can be written in the form

$$\begin{aligned}\mathbb{T}&=\frac{1}{2}\sum_{i=1}^{ne}\dot{\mathbf{d}}^T\mathbf{m}\,\dot{\mathbf{d}},\\ \text{with}\quad \mathbf{m}&=\mathbf{m}_{uu}+\mathbf{m}_{ww}+\mathbf{m}_{u\theta}+\mathbf{m}_{\theta\theta}\end{aligned} \tag{26}$$

in which

$$\begin{aligned}\mathbf{m}_{ww}&=\frac{l}{2}\int_{-1}^{1}\mathbf{N}_w^T\left[I_{11}^{C1M1}-I_{11}^{C12M12}\left(\frac{\xi+1}{2}\right)^{n_x}\right]\mathbf{N}_w\,d\xi,\\ \mathbf{m}_{u\theta}&=-\frac{l}{2}\int_{-1}^{1}\mathbf{N}_u^T\left[I_{12}^{C1M1}-I_{12}^{C12M12}\left(\frac{\xi+1}{2}\right)^{n_x}\right]\mathbf{N}_\theta\,d\xi,\\ \mathbf{m}_{\theta\theta}&=\frac{l}{2}\int_{-1}^{1}\mathbf{N}_\theta^T\left[I_{22}^{C1M1}-I_{22}^{C12M12}\left(\frac{\xi+1}{2}\right)^{n_x}\right]\mathbf{N}_\theta\,d\xi\end{aligned} \tag{27}$$

are, respectively, the element mass matrices resulted from the axial and transverse translations, axial translation-rotation coupling and cross-sectional rotation. Eq. (27) has been written by using Eq. (13) and notations $I_{11}^{C12M12}=I_{11}^{C1M1}-I_{11}^{C2M2}$, $I_{12}^{C12M12}=I_{12}^{C1M1}-I_{12}^{C2M2}$ and $I_{22}^{C12M12}=I_{22}^{C1M1}-I_{22}^{C2M2}$. The exact variation of the cross-sectional profile is also employed to compute the element mass matrices in Eq. (27).

Using the derived stiffness and mass matrices, the equations of motion for the free vibration analysis can be written in the form

$$\mathbf{M}\ddot{\mathbf{D}}+\mathbf{K}\mathbf{D}=\mathbf{0} \tag{28}$$

where $\mathbf{D}$, $\mathbf{M}$ and $\mathbf{K}$ are the global nodal displacement vector, mass and stiffness matrices, obtained by assembling the corresponding element vector and matrices over the total elements, respectively.

Table 1 Properties of constituent materials of BFGM beam (Nguyen *et al*. 2017)

Material	Role	E (GPa)	ρ (kg/m^3)	υ
Steel (SUS304)	M1	210	7800	0.3
Aluminum (Al)	M2	70	2702	0.23
Alumina (Al_2O_3)	C1	390	3960	0.3
Zirconia (ZrO_2)	C2	200	5700	0.3

Assuming a harmonic response for the free vibration, Eq. (28) leads to

$$(\mathbf{K}-\omega^2\mathbf{M})\bar{\mathbf{D}}=\mathbf{0} \tag{29}$$

with ω is the circular frequency, and $\bar{\mathbf{D}}$ is the vibration amplitude. Eq. (29) leads to an eigenvalue problem, which can be solved by the standard method (Cook *et al*. 2002).

4. Numerical results and discussion

Numerical investigations are carried out in this Section to study the effects of the material distribution and the tapered ratio on vibration characteristics of the BFGM beam. To this end, the beam is assumed to be formed from stainless steel (SUS304), aluminum (Al), alumina (Al_2O_3) and zirconium oxide (ZrO_2) with the material properties given in Table 1. Otherwise stated, an aspect ratio L/h_0 = 20

Table 2 Comparison of the fundamental frequency parameter of tapered unidirectional axial FGM beam with the result of Shahba *et al*. 2011) (n_x = 2)

			Taper ratio α							
B.C.	Case	Source	0.2	0.3	0.4	0.5	0.6	0.7	0.8	0.9
C-F	B	Shahba *et al*. (2011)	3.9956	4.0640	4.1438	4.2393	4.3571	4.5090	4.7180	5.0371
		Present	3.9955	4.0638	4.1434	4.2386	4.3560	4.5074	4.7154	5.0330
	C	Shahba *et al*. (2011)	4.2384	4.4565	4.7121	5.0178	5.3931	5.8695	6.5009	7.3787
		Present	4.2382	4.4560	4.7113	5.0164	5.3909	5.8660	6.4952	7.3696
S-S	B	Shahba et al.(2011)	7.2921	6.8975	6.4653	5.9879	5.4540	4.8448	4.1244	3.2016
		Present	7.2913	6.8963	6.4635	5.9854	5.4503	4.8394	4.1159	3.1858
	C	Shahba *et al*. (2011)	7.2245	6.7764	6.2755	5.7118	5.0709	4.3295	3.4452	2.3193
		Present	7.2235	6.7748	6.2730	5.7082	5.0655	4.3215	3.4326	2.2958
C-C	B	Shahba et al.(2011)	12.2126	11.9172	11.5739	11.1706	10.6896	10.1036	9.3634	8.3590
		Present	12.2114	11.9155	11.5715	11.1670	10.6843	10.0950	9.3483	8.3253
	C	Shahba *et al*. (2011)	12.2429	11.9737	11.6683	11.3199	10.9200	10.4579	9.9207	9.3010
		Present	12.2416	11.9718	11.6653	11.3153	10.9129	10.4466	9.9015	9.2639

Table 3 Comparison of the fundamental frequency parameter μ_1 of S-S uniform BFGM beam with the result of Nguyen *et al*. (2017)

n_z		n_x							
	Source	0	1/3	1/2	5/6	1	4/3	3/2	2
0	Nguyen *et al*. (2017)	3.3018	3.7429	3.9148	4.1968	4.3139	4.5118	4.5956	4.8005
	Present	3.3018	3.7428	3.9146	4.1966	4.3137	4.5116	4.5954	4.8003
1/3	Nguyen *et al*. (2017)	3.1542	3.5050	3.6305	3.8252	3.9022	4.0277	4.0792	4.2009
	Present	3.1542	3.5049	3.6304	3.8250	3.9021	4.0275	4.0790	4.2007
1/2	Nguyen *et al*. (2017)	3.1068	3.4285	3.5397	3.7087	3.7745	3.8805	3.9236	4.0245
	Present	3.1068	3.4284	3.5396	3.7085	3.7744	3.8803	3.9234	4.0243
5/6	Nguyen *et al*. (2017)	3.0504	3.3296	3.4206	3.5548	3.6059	3.6869	3.7194	3.7947
	Present	3.0504	3.3295	3.4205	3.5546	3.6057	3.6867	3.7192	3.7945
1	Nguyen *et al*. (2017)	3.0359	3.2984	3.3819	3.5035	3.5495	3.6219	3.6508	3.7177
	Present	3.0359	3.2983	3.3818	3.5034	3.5493	3.6217	3.6507	3.7176

is employed in all the computations reported below. Three types of boundary conditions (B.C.), namely clamped at x = 0 and free at $x = L$ (C-F), simply supported at both end (S-S), and clamped at both ends (C-C) are considered. In order to facilitate the discussion, the frequency parameters defined as $\mu_i = \omega_i \frac{L^2}{h}\sqrt{\rho_{M_1}/E_{M_1}}$ with ω_i is the i^{th} natural frequency; ρ_{M_1}, E_{M_1} are the elastic modulus and mass density of Al is introduced herewith.

4.1 Accuracy and convergence studies

The accuracy of the finite element model is shown by comparing the first frequency parameter of a tapered unidirectional axial FGM beam with the results of Shahba *et al*. (2011) in Table 2. The frequency parameter in the table is obtained for the beam formed from Al and ZrO_2 with a length $L = \sqrt{\frac{I_0}{0.01A_0}}$, and it is defined according to Shahba *et al*. (2011) as $\bar{\mu} = \sqrt{\frac{\rho_z L^4 A_0}{E_z I_0}}$, where ρ_Z and E_Z are, respectively, the mass density and Young's modulus of ZrO_2. Table 3 compares the fundamental frequency parameter of a S-S uniform BFGM beam with the results of Nguyen *et al*. (2017). Very good agreement between the frequency parameters obtained in the present work with that of Shahba *et al*. (2011) and Nguyen *et al*. (2017) is seen from Tables 2 and 3. Noting that both the referenced papers employed the first-order shear deformable beam elements with super convergent shape functions derived by Kosmatka (1995) to interpolate the transverse displacement and rotation in evaluating the fundamental frequency.

The convergence of the derived finite element formulation in evaluating the frequency parameter of a simply supported tapered BFGM with various values of the grading indexes and tapered ratio is illustrated in Table 4.

The convergence of the present formulation is achieved by using 30 elements, which is almost the same as that of

Table 4 Convergence of the formulation in evaluating frequency parameter $\mu_1$of S-S tapered BFGM beam (case C)

α	Grading indexes	Number of elements (*ne*)						
		10	15	20	25	30	35	40
0	$n_x = n_z = 1/2$	3.5401	3.5398	3.5397	3.5396	3.5396	3.5396	3.5396
	$n_x = n_z = 5/6$	3.5553	3.5549	3.5548	3.5547	3.5546	3.5546	3.5546
	$n_x = n_z = 1$	3.5500	3.5496	3.5494	3.5493	3.5493	3.5493	3.5493
0.2	$n_x = n_z = 1/2$	3.1423	3.1420	3.1419	3.1418	3.1418	3.1418	3.1418
	$n_x = n_z = 5/6$	3.1491	3.1487	3.1486	3.1485	3.1484	3.1484	3.1484
	$n_x = n_z = 1$	3.1428	3.1423	3.1422	3.1421	3.1420	3.1420	3.1420
0.6	$n_x = n_z = 1/2$	2.1602	2.1597	2.1596	2.1596	2.1596	2.1596	2.1596
	$n_x = n_z = 5/6$	2.1482	2.1476	2.1474	2.1473	2.1472	2.1472	2.1472
	$n_x = n_z = 1$	2.1389	2.1383	2.1381	2.1380	2.1379	2.1379	2.1379
0.9	$n_x = n_z = 1/2$	1.0178	1.0162	1.0154	1.0151	1.0149	1.0149	1.0149
	$n_x = n_z = 5/6$	0.9930	0.9912	0.9904	0.9900	0.9898	0.9898	0.9898
	$n_x = n_z = 1$	0.9818	0.9800	0.9791	0.9787	0.9785	0.9785	0.9785

the element using Kosmatka's shape functions (Kosmatka 1995) reported by Shahba *et al*. (2011). In this regards, a mesh of 30 elements is employed in the computations reported below.

4.2 Effect of material distribution

A BFGM beam of case B tapered type with a taper ratio α = 0.5 is considered in this subsection. Tables 5-7 list the fundamental frequency parameter μ_1 of the C-F, S-S and C-C beams for various values of the grading indexes n_x and n_z, respectively. The effect of the material distribution defining through the grading indexes n_x and n_z on the frequency parameter is clearly seen from the tables. At a given value of n_z, the tables show an increase of μ_1 by increasing the longitudinal index n_x, regardless of the boundary conditions.

Examining the table in more detail one can see that the variation of the parameter μ_1 with the increase of index n_x, however depends on the value of the index n_z, and this increase is less significant for the beam associated with a higher index n_z. For example, when increasing n_x from 0 to 2, μ_1 increases 42.19% for the C-F beam associated with n_z = 0.2, but this parameter increases only 39.74% and 36.9% for the beam having n_z = 1 and n_z = 2, respectively.

Table 5 Fundamental frequency parameter of C-F beam with various grading indexes

n_z	n_x						
	0	0.2	0.5	1	1.2	1.5	2
0	1.2825	1.4527	1.5965	1.7253	1.7582	1.7966	1.8422
0.2	1.2445	1.4181	1.5587	1.6767	1.7048	1.7358	1.7695
0.5	1.2066	1.3868	1.5255	1.6331	1.6562	1.6799	1.7021
1	1.1792	1.3689	1.5064	1.6030	1.6210	1.6372	1.6478
1.2	1.1756	1.3681	1.5051	1.5983	1.6149	1.6289	1.6363
1.5	1.1743	1.3701	1.5062	1.5951	1.6098	1.6211	1.6246
2	1.1781	1.3772	1.5116	1.5945	1.6067	1.6145	1.6130

The boundary conditions also play an important role on the dependence of μ_1 with the longitudinal index. The frequency parameter μ_1 increases 19.53% and 18.73%, respectively, for the S-S beam and C-C beam with n_z = 1 when increasing n_x from 0 to 2, which is much lower comparing to that of the C-F beam. The increase of the frequency parameter can be explained by the higher content of the ceramics for a beam associated with a higher index

Table 6 Fundamental frequency parameter of S-S beam with various grading indexes

n_z	n_x						
	0	0.2	0.5	1	1.2	1.5	2
0	2.3869	2.5653	2.7789	3.0465	3.1319	3.2426	3.3901
0.2	2.3161	2.4686	2.6424	2.8493	2.9131	2.9943	3.1005
0.5	2.2457	2.3725	2.5085	2.6623	2.7084	2.7664	2.8412
1	2.1945	2.2945	2.3940	2.5011	2.5326	2.5721	2.6230
1.2	2.1877	2.2795	2.3688	2.4638	2.4917	2.5267	2.5720
1.5	2.1855	2.2665	2.3429	2.4234	2.4471	2.4770	2.5159
2	2.1925	2.2583	2.3177	2.3801	2.3988	2.4226	2.4541

Table 7 Fundamental frequency parameter of C-C beam with various grading indexes

n_z	n_x						
	0	0.2	0.5	1	1.2	1.5	2
0	5.4376	6.0099	6.5160	7.0321	7.1834	7.3750	7.6277
0.2	5.2779	5.8078	6.2309	6.6122	6.7145	6.8391	6.9964
0.5	5.1191	5.6104	5.9531	6.2119	6.2726	6.3422	6.4251
1	5.0034	5.4571	5.7196	5.8663	5.8913	5.9157	5.9406
1.2	4.9880	5.4301	5.6697	5.7865	5.8026	5.8159	5.8271
1.5	4.9826	5.4087	5.6194	5.7004	5.7060	5.7064	5.7020
2	4.9979	5.4000	5.5725	5.6088	5.6016	5.5870	5.5644

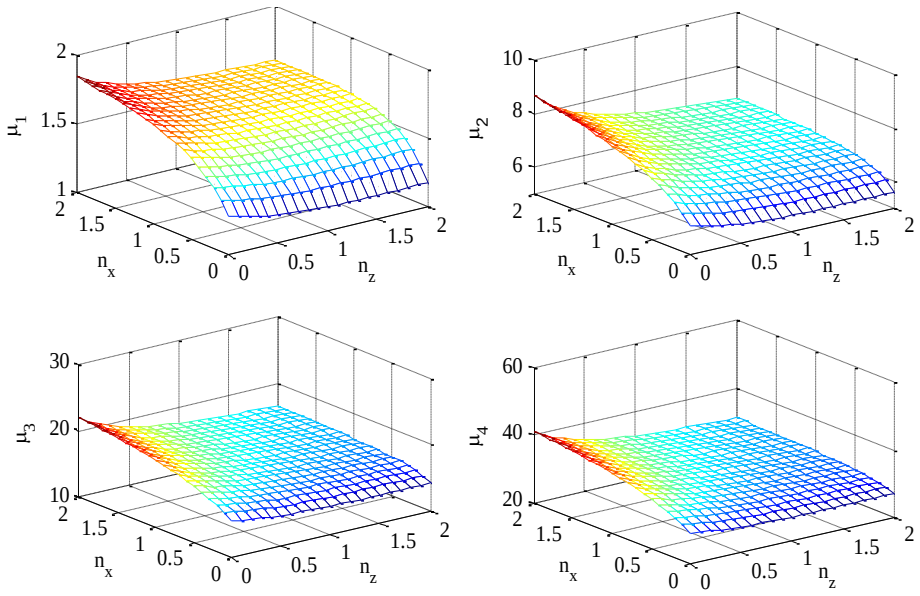

Fig. 3 Variation of the first four natural frequencies with grading indexes of C-F beam

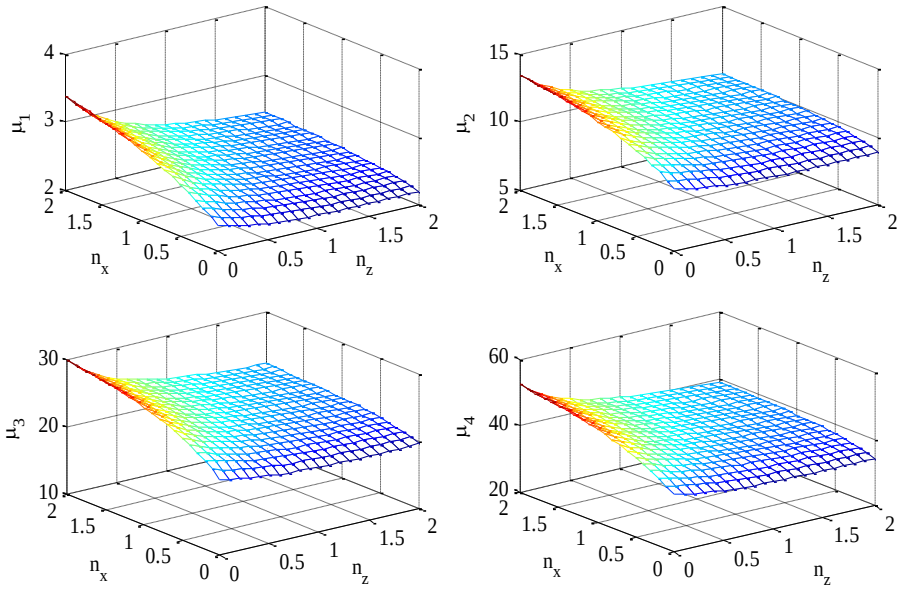

Fig. 4 Variation of the first four natural frequencies with grading indexes of S-S beam

n_x, as can be seen from Eq. (2), and this leads to higher rigidities of the beam. The mass moments of the beam with a higher index n_x are also larger, but with the material data in Table 1, the increase of the rigidities by increasing n_x is more significant than that of the mass moments, and this explains for the increase of the frequency by increasing the index n_x. The effect of the index n_z on the frequency parameter is, however opposite to that of the index n_x, and the frequency parameter decrease by the increase of n_z, regardless of the boundary condition. The change of the parameter μ_1 by the change of n_z is also dependent on the index n_x, and the decrease of μ_1 by increasing n_z is more significant for the beam with a higher index n_x. The decrease of the parameter μ_1 by the increase of n_z can also be explained by the more significant decrease of the rigidities comparing the increase of the mass moments for the beam associated with a higher index n_z. Among the three boundary conditions considered herein the C-F is the most sensitive to the change of the material grading indexes and the C-C beam is the least sensitive to the change of these parameters.

Figs. 3-5 depict the variation of the first four frequency parameters with the grading indexes n_x and n_z of the C-F, S-S and C-C beams, respectively. The variation of the second, third and fourth frequency parameter with the material grading indexes, as can be seen from the figures, is similar to that of the first frequency parameter, that is they also increase with increasing n_x and decrease when increasing n_z, regardless of the boundary conditions. The variation of the frequencies with the grading indexes in the figures guides to design a tapered BFGM beam with desired frequencies by appropriately choosing the material grading indexes.

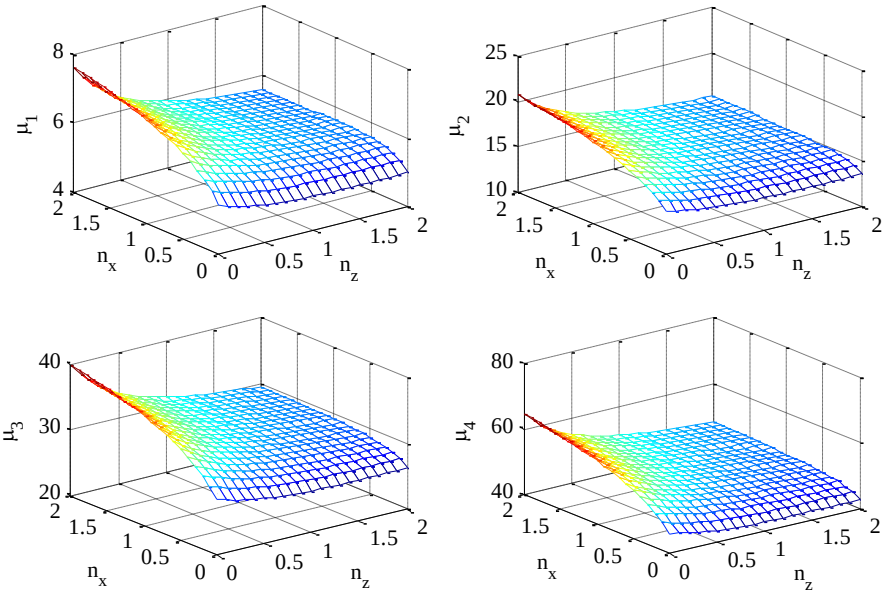

Fig. 5 Variation of the first four natural frequencies with grading indexes of C-C beam

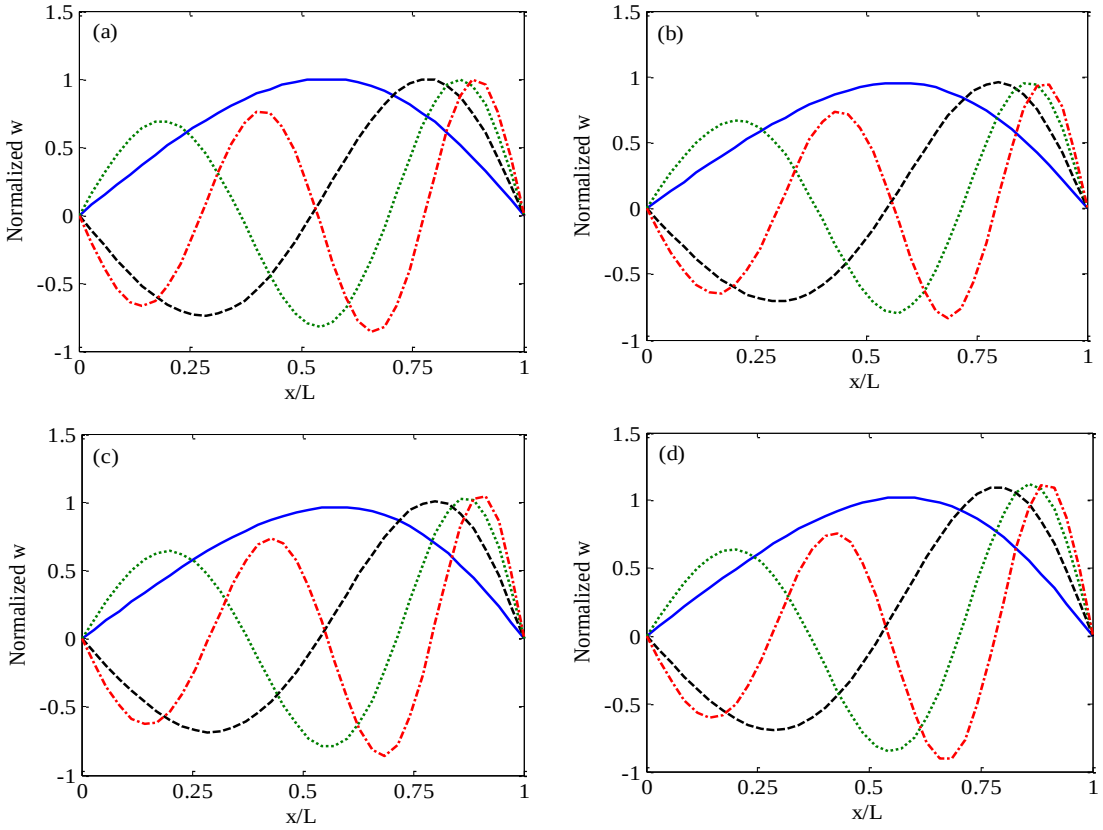

Fig. 6 Vibration mode shapes for transverse displacement of S-S beam with different grading indexes: (a) $n_x = 0$, $n_z = 0.5$; (b) $n_x = 0.5$, $n_z = 0$; (c) $n_x = 2$, $n_z = 0.5$; (d) $n_x = 0.5$, $n_z = 2$

The first four mode shapes for the transverse displacement of the simply supported BFGM beam are illustrated in Fig. 6 for various values of the grading indexes n_x and n_z. As can be seen from the figure that the flexural mode shapes of the BFGM beam are different from that of the conventional transverse FGM beam, and the first mode is no longer symmetric with respect to the mid-span of the beam. The effect of the grading indexes which define the material distribution on the flexural mode shapes of the BFGM beam is clearly seen from the figure.

4.3 Effect of taper ratio and taper case

The taper ratio versus the fundamental frequency

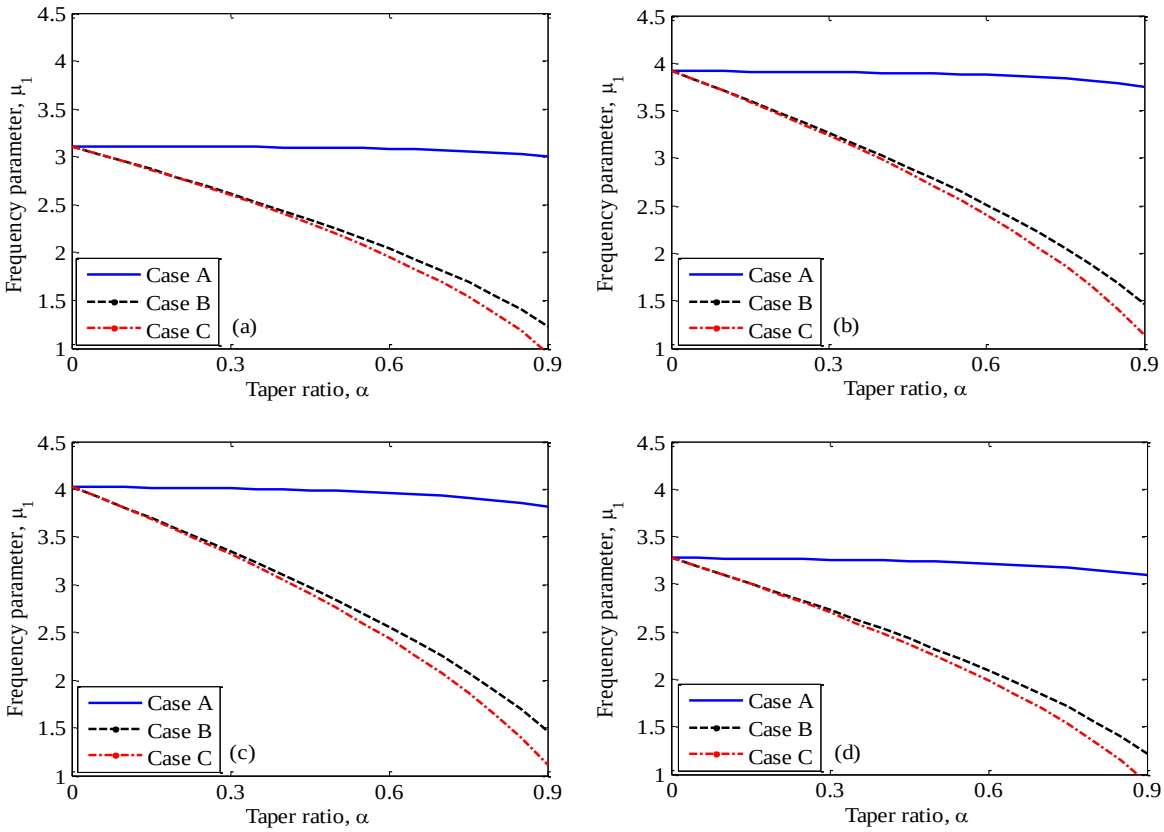

Fig. 8 Taper ratio versus fundamental frequency parameter of S-S beam with different taper cases and grading indexes: (a) $n_x = 0$, $n_z = 0.5$; (b) $n_x = 0.5$, $n_z = 0$; (c) $n_x = 2$, $n_z = 0.5$; (d) $n_x = 0.5$, $n_z = 2$

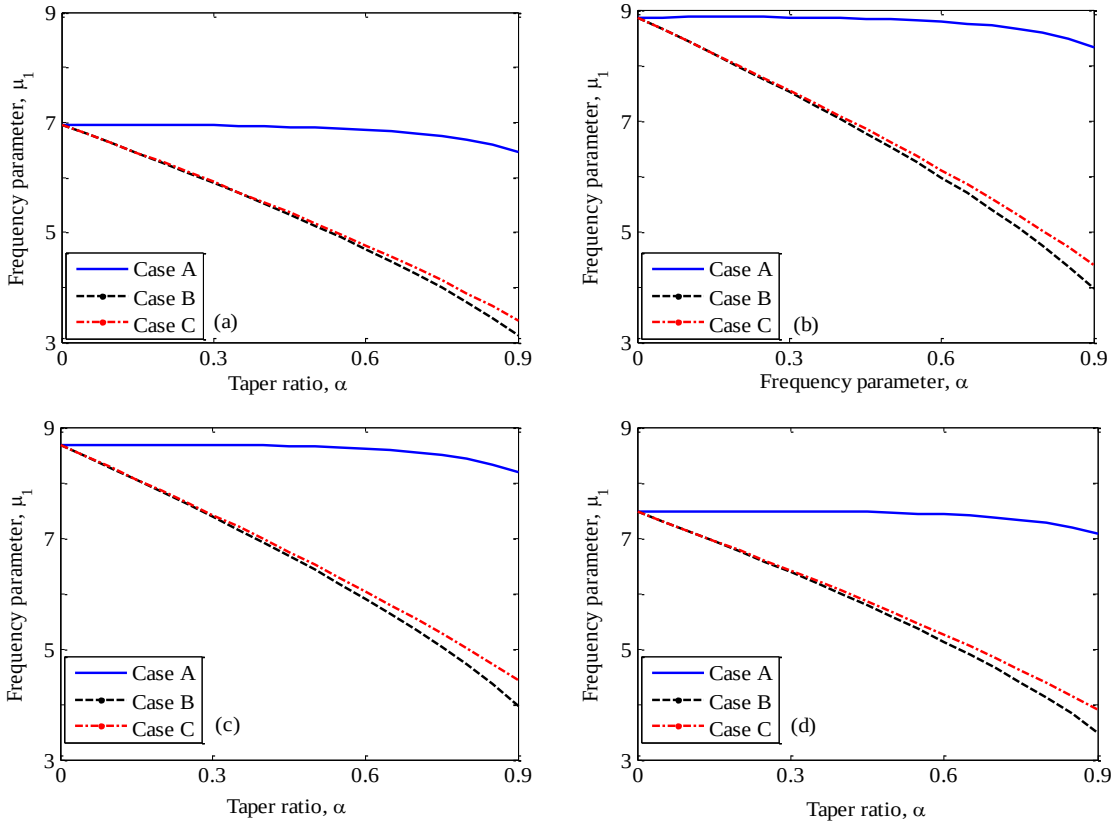

Fig. 9 Taper ratio versus fundamental frequency parameter of C-C beam with different taper cases and grading indexes: (a) $n_x = 0$, $n_z = 0.5$; (b) $n_x = 0.5$, $n_z = 0$; (c) $n_x = 2$, $n_z = 0.5$; (d) $n_x = 0.5$, $n_z = 2$

Table 8 Frequency parameter μ_1 of case B tapered C-F beam with different aspect ratios

L/h_0	α	n_z	n_x						
			0	0.2	0.5	1	1.2	1.5	2
5	0	0	1.1455	1.3118	1.4461	1.5596	1.5875	1.6193	1.6564
		0.5	1.0798	1.2565	1.3858	1.4789	1.4975	1.5157	1.5315
		1	1.0555	1.2417	1.3695	1.4519	1.4658	1.4770	1.4823
		1.5	1.0508	1.2429	1.3692	1.4442	1.4550	1.4618	1.4606
		2	1.0535	1.2489	1.3735	1.4429	1.4513	1.4550	1.4494
	0.5	0	1.2526	1.4177	1.5577	1.6838	1.7162	1.7541	1.7992
		0.5	1.1804	1.3546	1.4888	1.5933	1.6159	1.6391	1.6610
		1	1.1537	1.3367	1.4693	1.5626	1.5801	1.5958	1.6063
		1.5	1.1486	1.3371	1.4679	1.5535	1.5677	1.5787	1.5821
		2	1.1517	1.3431	1.4721	1.5517	1.5635	1.5710	1.5696
10	0	0	1.1719	1.3435	1.4815	1.5973	1.6255	1.6576	1.695
		0.5	1.1031	1.2859	1.4194	1.5150	1.5340	1.5524	1.5682
		1	1.0780	1.2711	1.4035	1.4885	1.5027	1.5140	1.5192
		1.5	1.0735	1.2731	1.4043	1.4818	1.4928	1.4997	1.4982
		2	1.0768	1.2801	1.4097	1.4815	1.4901	1.4937	1.4877
	0.5	0	1.2764	1.4455	1.5885	1.7167	1.7495	1.7878	1.8333
		0.5	1.2012	1.3802	1.518	1.6249	1.6479	1.6715	1.6936
		1	1.1739	1.3623	1.4987	1.5946	1.6126	1.6286	1.6392
		1.5	1.1690	1.3633	1.4983	1.5865	1.6011	1.6123	1.6158
		2	1.1727	1.3702	1.5034	1.5856	1.5978	1.6055	1.6040
15	0	0	1.1771	1.3497	1.4884	1.6047	1.6329	1.6651	1.7025
		0.5	1.1076	1.2916	1.4260	1.5220	1.5411	1.5596	1.5754
		1	1.0824	1.2768	1.4102	1.4956	1.5099	1.5213	1.5264
		1.5	1.0779	1.2790	1.4111	1.4892	1.5002	1.5071	1.5055
		2	1.0813	1.2861	1.4167	1.4890	1.4977	1.5013	1.4952
	0.5	0	1.2809	1.4509	1.5944	1.7231	1.7559	1.7943	1.8399
		0.5	1.2052	1.3851	1.5236	1.6309	1.6541	1.6777	1.6999
		1	1.1778	1.3672	1.5044	1.6008	1.6188	1.6350	1.6456
		1.5	1.1730	1.3684	1.5041	1.5929	1.6076	1.6188	1.6223
		2	1.1767	1.3754	1.5095	1.5922	1.6044	1.6122	1.6106

parameter of the BFGM beam with n_z = 0.5 and different values of n_x is depicted in Figs. 7-9 for the C-F, S-S and C-C beams, respectively. As can be seen from the figures, the variation of the frequency parameter with the taper ratio is governed by the boundary condition and the taper case as well. While the frequency parameter of the C-F beam increases by increasing the taper ratio, that of the S-S and C-C beams decreases with the increase of the taper ratio, regardless of the taper case. For a given boundary condition, the dependence of the frequency parameter upon the taper ratio α is, however significantly influenced by the taper case. The rate of the variation of μ_1 with α is the most significant for the type C of the C-F and S-S beams, while that is occurred for the type B of the C-C beam.

4.4 Effect of aspect ratio

The effect of the aspect ratio L/h_0 on the frequencies of the frequency of the BFGM beams is illustrated in Tables 8 and 9, where the fundamental frequency parameters of the C-F and S-S beams are, respectively, given for different values of the aspect ratio and the grading indexes. The frequency parameter μ_1 is increased with an increase of the aspect ratio, regardless of the grading indexes and the boundary condition. A careful examination of the tables shows that the effect of the aspect ratio on the frequency of the tapered beam is less significant than that of the uniform beam. For example, with n_x = 1 and n_z = 1 the frequency parameter of the uniform C-F beam increases 3.01% when increasing the aspect ratio from 5 to 15, while that of tapered C-F beam with α = 0.5 increases only 2.44%. The effect of the aspect ratio on the frequency is also influenced by the boundary condition, and the increase of the fundamental frequency of the S-S beam is more significant than that of the C-F beam, regardless of the grading indexes and the taper ratio. The effect of the aspect ratio obtained in

Table 9 Frequency parameter μ_1 of case B tapered S-S beam with different aspect ratios

L/h_0	α	n_z	n_x						
			0	0.2	0.5	1	1.2	1.5	2
5	0	0	3.1157	3.3872	3.6942	4.0608	4.1740	4.3179	4.5048
		0.5	2.9395	3.1436	3.3465	3.5597	3.6201	3.6937	3.7843
		1	2.8706	3.0413	3.1957	3.3460	3.3868	3.4356	3.4946
		1.5	2.8545	3.0020	3.1259	3.2402	3.2705	3.3065	3.3496
		2	2.8592	2.9880	3.0896	3.1796	3.2031	3.2310	3.2643
	0.5	0	2.3076	2.4821	2.6876	2.9429	3.0240	3.1290	3.2688
		0.5	2.1747	2.2978	2.4274	2.5726	2.6159	2.6704	2.7406
		1	2.1246	2.2213	2.3154	2.4156	2.4449	2.4817	2.5291
		1.5	2.1142	2.1925	2.2643	2.3388	2.3607	2.3882	2.4242
		2	2.1191	2.1828	2.2382	2.2954	2.3124	2.3341	2.3630
10	0	0	3.2613	3.5422	3.8666	4.2585	4.3800	4.5346	4.7355
		0.5	3.0705	3.2820	3.4977	3.7276	3.7932	3.8733	3.9718
		1	3.0001	3.1765	3.3414	3.5050	3.5499	3.6037	3.6688
		1.5	2.9866	3.1383	3.2711	3.3969	3.4307	3.4709	3.5193
		2	2.9950	3.1266	3.2358	3.3360	3.3627	3.3943	3.4323
	0.5	0	2.3702	2.5479	2.7597	3.0248	3.1093	3.2187	3.3646
		0.5	2.2308	2.3569	2.4916	2.6435	2.6890	2.7463	2.8200
		1	2.1799	2.2792	2.3775	2.4832	2.5142	2.5531	2.6033
		1.5	2.1705	2.2510	2.3264	2.4057	2.4290	2.4583	2.4966
		2	2.1771	2.2425	2.3011	2.3624	2.3807	2.4040	2.4349
15	0	0	3.2911	3.5740	3.9020	4.2992	4.4224	4.5794	4.7832
		0.5	3.0972	3.3102	3.5285	3.7620	3.8287	3.9101	4.0104
		1	3.0264	3.2040	3.3711	3.5376	3.5834	3.6383	3.7047
		1.5	3.0136	3.1661	3.3008	3.4290	3.4636	3.5048	3.5542
		2	3.0228	3.1550	3.2658	3.3682	3.3955	3.4280	3.4670
	0.5	0	2.3825	2.5608	2.7739	3.0408	3.1260	3.2363	3.3835
		0.5	2.2418	2.3684	2.5041	2.6574	2.7034	2.7611	2.8356
		1	2.1907	2.2905	2.3897	2.4964	2.5278	2.5671	2.6178
		1.5	2.1816	2.2625	2.3386	2.4187	2.4424	2.4721	2.5108
		2	2.1885	2.2541	2.3134	2.3755	2.3940	2.4177	2.4491

this subsection shows the ability of the finite element model developed in this paper in modeling the shear deformation effect on the frequencies of the BFGM beams.

5. Conclusions

An efficient finite element model has been formulated and employed to study the free vibration of BFGM beams. The model has been derived by using the hierarchical functions to interpolate the displacements and rotation of the beams. To improve the efficiency and accuracy of the element model, the shear strain was enforced to constant and the exact variation of the cross-sectional profile was employed to compute the element stiffness and mass matrices. Numerical investigations revealed that the finite element model proposed in the present paper is efficient, and it is capable to give accurate natural frequencies of BFGM beams by using a small number of the elements. A parametric study has been carried out to illustrate the effect of the material distribution, taper ratio and boundary conditions on the vibration characteristics. The obtained numerical results showed that the dependence of the fundamental frequency upon the taper ratio is significantly influenced by the taper type and the boundary conditions of the beams. The present results are of benefit to optimum design of tapered BFGM beams. It should be noted that the finite element model in the present paper was derived for the beams with the three tapered cases, and more efforts are necessary to make for dealing with BFGM beams with more complicated variation of cross section.

Acknowledgments

This work was supported by Vietnam National Foundation for Science and Technology Development (NAFOSTED) under Grant no. 107.02-2018.23.

References

Akgöz, B. and Civalek, Ö. (2013), "Free vibration analysis of axially functionally graded tapered Bernoulli–Euler microbeams based on the modified couple stress theory", *Compos. Struct.*, **98**, 314-322.

Bambill, D.V., Rossit, C.A. and Felix, D.H. (2015), "Free vibrations of stepped axially functionally graded Timoshenko beams", *Meccanica*, **50**(4), 1073-1087.

Birman, V. and Byrd, L.W. (2007), "Modeling and Analysis of functionally graded materials and structures", *Appl. Mech. Rev.*, **60**(5), 195-216.

Calim, F.F. (2016), "Transient analysis of axially functionally graded Timoshenko beams with variable cross-section", *Compos. Part B*, **98**, 472-483.

Chakraborty, A., Gopalakrishnan, S. and Reddy, J.N. (2003), "A new beam finite element for the analysis of functionally graded materials", *Int. J. Mech. Sci.*, **45**(3), 519-539.

Cook, R.D., Malkus, D.S., Plesha, M.E. and Witt, R.J. (2002), *Concepts and Applications of Finite Element Analysis*, (4th Ed.), John Wiley & Sons, New York, NY, USA.

Frikha, A., Hajlaoui, A., Wali, M. and Dammak, F. (2016), "A new higher order C^0 mixed beam element for FGM beams analysis", *Compos. Part B Eng.*, **106**, 181-189.

Gan, B.S., Trinh, T.H., Le, T.H. and Nguyen, D.K. (2015), "Dynamic response of non-uniform Timoshenko beams made of axially FGM subjected to multiple moving point loads", *Struct. Eng. Mech., Int. J.*, **53**(5), 981-995.

Ghazaryan, D., Burlayenko, V.N., Avetisyan, A. and Bhaskar, A. (2017), "Free vibration analysis of functionally graded beams with non-uniform cross-section using the differential transform method", *J. Eng. Math.*, DOI: 10.1007/s10665-017-9937-3

Hao, D. and Wei, C. (2016), "Dynamic characteristics analysis of bi-directional functionally graded Timoshenko beams", *Compos. Struct.*, **141**, 253-263.

Hein, H. and Feklistova, L. (2011), "Free vibrations of non-uniform and axially functionally graded beams using Haar wavelets", *Eng. Struct.*, **33**(12), 3696-3701.

Huang, Y. and Li, X.-F. (2010), "A new approach for free vibration of axially functionally graded beams with non-uniform cross-section", *J. Sound Vib.*, **329**(11), 2291-2303.

Huang, Y. and Li, X.-F. (2011), "Buckling analysis of nonuniform and axially graded columns with varying flexural rigidity", *ASCE J. Eng. Mech.*, **137**(1), 73-81.

Huang, Y., Yang, L.-E. and Luo, Q.-Z. (2013), "Free vibration of axially functionally graded Timoshenko beams with non-uniform cross-section", *Compos. Part B Eng.*, **45**(1), 1493-1498.

Huynh, T.A., Lieu, X.Q. and Lee, J. (2017), "NURBS-based modeling of bidirectional functionally graded Timoshenko beams for free vibration problem", *Compos. Struct.*, **160**, 1178-1190.

Kadoli, R., Akhtar, K. and Ganesan, N. (2008), "Static analysis of functionally graded beams using higher order shear deformation theory", *Appl. Math. Model.*, **32**(12), 2509-2525.

Kahya, V. and Turan, M. (2017), "Finite element model for vibration and buckling of functionally graded beams based on the first-order shear deformation theory", *Compos. Part B Eng.*, **109**, 108-115.

Karamanli, A. (2017), "Bending behaviour of two directional functionally graded sandwich beams by using a quasi-3d shear deformation theory", *Compos. Struct.*, **174**, 70-86.

Kosmatka, J.B. (1995), "An improved two-node finite element for stability and natural frequencies of axial-loaded Timoshenko beams", *Comput. Struct.*, **57**(1), 141-149.

Lezgy-Nazargah, M. (2015), "Fully coupled thermo-mechanical analysis of bi-directional FGM beams using NURBS isogeometric finite element approach", *Aerosp. Sci. Technol.*, **45**, 154-164.

Li, X.-F. (2008), "A unified approach for analyzing static and dynamic behaviours of functionally graded Timoshenko and Euler-Bernoulli beams", *J. Sound Vib.*, **318**(4-5), 1210-1229.

Li, X.-F., Kang, Y.-A. and Wu, J.-X. (2013), "Exact frequency equations of free vibration of exponentially functionally graded beams", *App. Acoust.*, **74**(3), 413-420.

Li, L. and Zhang, D. (2015), "Dynamic analysis of rotating axially FG tapered beams based on a new rigid-flexible coupled dynamic model using the B-spline method", *Compos. Struct.*, **124**, 357-367.

Lü, C.F., Chen, W.Q., Xu, R.Q. and Lim, C.W. (2008), "Semi-analytical elasticity solutions for bi-directional functionally graded beams", *Int. J. Solids Struct.*, **45**, 258-275.

Mahi, A., Adda Bedia, E.A., Tounsi, A. and Mechab, I. (2010), "An analytical method for temperature-dependent free vibration analysis of functionally graded beams with general boundary conditions", *Compos. Struct.*, **92**(8), 1877-1887.

Nguyen, D.K. (2013), "Large displacement response of tapered cantilever beams made of axially functionally graded material", *Compos. Part B Eng.*, **55**, 298-305.

Nguyen, D.K. and Gan, B.S. (2014), "Large deflections of tapered functionally graded beams subjected to end forces", *Appl. Math. Model.*, **38**(11-12), 3054-3066.

Nguyen, D.K. and Bui, V.T. (2017), "Dynamic analysis of functionally graded Timoshenko beams in thermal environment using a higher-order hierarchical beam element", *Math. Prob. Eng.* DOI: https://doi.org/10.1155/2017/7025750

Nguyen, D.K., Nguyen, Q.H., Tran, T.T. and Bui, V.T. (2017), "Vibration of bi-dimensional functionally graded Timoshenko beams excited by a moving load", *Acta Mech.*, **228**, 141-155.

Nemat-Alla, M. and Noda, N. (2000), "Edge crack problem in a semi-infinite FGM plate with a bi-directional coefficient of thermal expansion under two-dimensional thermal loading", *Acta Mech.*, **144**(3-4), 211-229.

Niknam, H., Fallah, A. and Aghdam, M.M. (2014), "Nonlinear bending of functionally graded tapered beams subjected to thermal and mechanical loading", *Int. J. Non-Linear Mech.*, **65**, 141-147.

Pydah, A. and Sabale, A. (2017), "Static analysis of bi-directional functionally graded curved beams", *Compos. Struct.*, **160**, 867-876.

Rajasekaran, S. (2013), "Buckling and vibration of axially functionally graded nonuniform beams using differential transformation based dynamic stiffness approach", *Meccanica*, **48**(5), 1053-1070.

Rajasekaran, S. and Tochaei, E.N. (2014), "Free vibration analysis of axially functionally graded tapered Timoshenko beams using differential transformation element method and differential quadrature element method of lowest-order", *Meccanica*, **49**(4), 995-1009.

Shahba, A. and Rajasekaran, S. (2012), "Free vibration and stability of tapered Euler–Bernoulli beams made of axially functionally graded materials", *App. Math. Model.*, **36**(7), 3094-3111.

Shahba, A., Attarnejad, R., Marvi, M.T. and Hajilar, S. (2011), "Free vibration and stability analysis of axially functionally graded tapered Timoshenko beams with classical and non-classical boundary conditions", *Compos. Part B Eng.*, **42**(4), 801-808.

Shafiei, N. and Kazemi, M. (2017), "Buckling analysis on the bi-dimensional functionally graded porous tapered nano-/micro-scale beams", *Aerosp. Sci. Technol.*, **66**, 1-11.

Shafiei, N., Mirjavadi, S.S., Afshari, B.M., Rabby, S. and Kazemi, M. (2017), "Vibration of two-dimensional imperfect functionally graded (2D-FG) porous nano-/micro-beams",

Comput. Method Appl. Mech. Eng., **322**, 615-632.

Şimşek, M. (2015), "Bi-directional functionally graded materials (BDFGMs) for free and forced vibration of Timoshenko beams with various boundary conditions", *Compos. Struct.*, **133**, 968-997.

Tang, A.-Y., Wu, J.-X., Li, X.-F. and Lee, K.Y. (2014), "Exact frequency equations of free vibration of exponentially non-uniform functionally graded Timoshenko beams", *Int. J. Mech. Sci.*, **89**, 1-11.

Trinh, L.C., Vo, P.T., Thai, H.T. and Nguyen, T.K. (2016), "An analytical method for the vibration and buckling of functionally graded beams under mechanical and thermal loads", *Compos. Part B Eng.*, **100**, 152-163.

Trinh, L.C., Vo, T.P., Thai, H-T. and Nguyen, T-K. (2018), "Size-dependent vibration of bi-directional functionally graded microbeams with arbitrary boundary conditions", *Compos. Part B Eng.*, **134**, 225-245.

Wang, Z., Wang, X., Xu, G., Cheng, S. and Zeng, T. (2016), "Free vibration of two-directional functionally graded beams", *Compos. Struct.*, **135**, 191-198.

Wattanasakulpong, N., Prusty, B.G. and Kelly, D.W. (2011), "Thermal buckling and elastic vibration of third-order shear deformable functionally graded beams", *Int. J. Mech. Sci.*, **53**(9), 734-743.

Zhao, Y., Huang, Y. and Guo, M. (2017), "A novel approach for free vibration of axially functionally graded beams with non-uniform cross-section based on Chebyshev polynomials theory", *Compos. Struct.*, **168**, 277-284.

Zienkiewicz, O.C. and Taylor, R.L. (1997), *The Finite Element Method*, *Vol. 1*: *Basic Formulation an Linear Problems*, (4th Ed.), Mc. Graw-Hill Book Company, London, UK.

CC